Biochemical and Structural Characterization of *Salmonella typhimurium* Glyoxalase II: New Insights into Metal Ion Selectivity[†,‡]

Valeria A. Campos-Bermudez,[§] Ney Ribeiro Leite,[||] Renata Krog,[||] Antonio J. Costa-Filho,[⊥] Fernando C. Soncini,[§] Glaucius Oliva,[||] and Alejandro J. Vila*[,§]

Instituto de Biología Molecular y Celular de Rosario, IBR-CONICET and Area Biofísica, Facultad de Ciencias Bioquímicas y Farmacéuticas, Universidad Nacional de Rosario, Rosario S2002LRK, Argentina, and Centro de Biotecnologia Molecular e Estrutural and Grupo de Biofisica Molecular Sérgio Mascarenhas, Instituto de Física de São Carlos, Universidade de São Paulo, CP 369, 13560-970 São Carlos, SP, Brazil

Received April 17, 2007; Revised Manuscript Received July 30, 2007

ABSTRACT: Glyoxalase II is a hydrolytic enzyme part of the glyoxalase system, responsible for detoxifying several cytotoxic compounds employing glutathione. Glyoxalase II belongs to the superfamily of metallo-β-lactamases, with a conserved motif able to bind up to two metal ions in their active sites, generally zinc. Instead, several eukaryotic glyoxalases II have been characterized with different ratios of iron, zinc, and manganese ions. We have expressed a gene coding for a putative member of this enzyme superfamily from *Salmonella typhimurium* that we demonstrate, on the basis of its activity, to be a glyoxalase II, named GloB. Recombinant GloB expressed in *Escherichia coli* was purified with variable amounts of iron, zinc, and manganese. All forms display similar activities, as can be shown from protein expression in minimal medium supplemented with specific metal ions. The crystal structure of GloB solved at 1.4 Å shows a protein fold and active site similar to those of its eukaryotic homologues. NMR and EPR experiments also reveal a conserved electronic structure at the metal site. GloB is therefore able to accommodate these different metal ions and to carry out the hydrolytic reaction with similar efficiencies in all cases. The metal promiscuity of this enzyme (in contrast to other members of the same superfamily) can be accounted for by the presence of a conserved Asp residue acting as a second-shell ligand that is expected to increase the hardness of the metal binding site, therefore favoring iron uptake in glyoxalases II.

Methylglyoxal is a cytotoxic and mutagenic compound that is formed primarily as a byproduct of carbohydrate and lipid metabolism (*1*, *2*). In *Escherichia coli*, endogenous methylglyoxal synthesis occurs when there is an imbalance between the rates of the lower segment of glycolysis, from glyceraldehyde 3-phosphate (PGAL)[1] to pyruvate, and the pathways generating dihydroxyacetone phosphate and PGAL (*3*, *4*). Methylglyoxal is able to modify DNA and protein residues, leading to the degradation of these essential components and subsequent apoptosis of the cells (*5*). The major means of protection against this harmful compound relies on its spontaneous reaction with glutathione, followed by detoxification through the glyoxalase system (Figure 1). The glyoxalase system consists of two enzymes, glyoxalase I (GLX1; EC 4.4.1.5, lactoylglutathione methylglyoxal lyase) and glyoxalase II (GLX2; EC 3.1.2.6, hydroxyacylglutathione hydrolase) (*1*, *3*). Aromatic and aliphatic α-keto aldehydes such as methylglyoxal react spontaneously with glutathione to form thiohemiacetals, and GLX1 catalyzes the isomerization of this thiohemiacetal to produce *S*-(2-hydroxyacyl)-glutathione derivatives (*6*−*8*). GLX2 hydrolyzes *S*-(2-hydroxyacyl)glutathione derivatives to regenerate glutathione, thus releasing harmless hydroxyacids (Figure 1) (*3*).

The glyoxalase system is present in different organisms, and so far, a series of studies on their constituent enzymes have revealed conserved structural features. GLX1 is a well-described metalloenzyme that requires one divalent metal ion in its active site essential for its activity (*6*−*8*). Despite a large sequence and structural similarity among the GLX1 family from different sources, they can be divided into

[†] This work was supported by grants from ANPCyT and HHMI to A.J.V. V.A.C.-B. is the recipient of a doctoral fellowship from CONICET. The Bruker Avance II 600 MHz NMR spectrometer was purchased with funds from ANPCyT (Grant No. PME2003-0026) and CONICET. A.J.V. and F.C.S. are staff members from CONICET. A.J.V. is an International Research Scholar of the Howard Hughes Medical Institute. The Centro de Biotecnologia Molecular Estrutural and NRL are supported by FAPESP. A.J.C.-F. thanks PRONEX/FAPESP/CNPq (Grant No. 03/09859-2) and CNPq (Grant No. 307102/ 2006-8) for financial support.

[‡] Coordinates for the structure discussed in this manuscript have been deposited in the Protein Data Bank under PDB code 2QED.

* To whom correspondence should be addressed. Phone: +54-341-4351235 ext 108. Fax: +54-341-4390465. E-mail: vila@ibr.gov.ar.

[§] Universidad Nacional de Rosario.

[||] Centro de Biotecnologia Molecular e Estrutural, Universidade de São Paulo.

[⊥] Grupo de Biofísica Molecular Sérgio Mascarenhas, Universidade de São Paulo.

[1] Abbreviations: GLX1, glyoxalase I; GLX2, glyoxalase II; PGAL, glyceraldehyde 3-phosphate; IPTG, isopropyl β-D-thiogalactoside; SLG, *S*-D-lactoylglutathione; DTNB, 5,5′-dithiobis(2-nitrobenzoate); MOPS, 3-(*N*-morpholino)propanesulfonic acid; GST, glutathione-*S*-transferase; PEG, polyethylene glycol; MES, 2-(*N*-morpholino)ethanesulfonic acid; EDTA, ethylenediaminetetraacetic acid; EPR, electronic paramagnetic resonance; NMR, nuclear magnetic resonance; rmsd, root mean square deviation.

10.1021/bi7007245 CCC: $37.00
Published on Web 09/01/2007

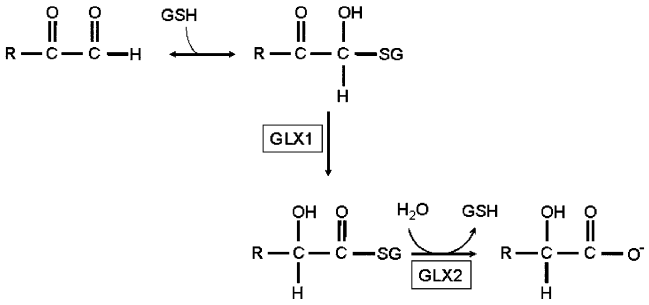

FIGURE 1: Mechanism of the glyoxalase system. The major means of protection against methylglyoxal is the spontaneous reaction of this compound with glutathione to form the hemithiolacetal, followed by detoxification by the glyoxalase system, leading to the production of D-lactate.

Zn(II)-dependent and Ni(II)-dependent enzymes. It has been shown that the metal ion selectivity within different GLX1 family members is finely controlled by the protein structure (*6*−*9*). GLX2 is also a metalloenzyme, but with quite different (and less explored) features in this respect. The first crystal structure available for a GLX2 was that of the human variant, reported as a dizinc enzyme, despite the observation of a nonnegligible iron content in the same sample (*10*). Later, other eukaryotic GLX2 enzymes were isolated and characterized in their zinc, iron, and manganese forms (*11*−*14*), since they are usually expressed in *E. coli* as mixed metal forms. While all these metal derivatives seem to be equally active, the in vivo metal requirements of these enzymes are still obscure.

GLX2 is one of many members characterized to date of the metallo-β-lactamase superfamily (*15*, *16*). Proteins belonging to this superfamily are characterized by the presence of an $\alpha\beta/\beta\alpha$ fold and a conserved motif able to bind up to two metal ions in their active sites (*17*, *18*). Metallo-β-lactamases and other hydrolases from the same superfamily (such as phosphodiesterase, acyl-homoserine-lactone lactonase, methylparathion hydrolase, and alkylsulfatase) (*19*−*24*) are zinc-dependent enzymes, while the terminal oxidase rubredoxin:oxygen oxidoreductase from *Desulfovibrio gigas* (ROO) is a diiron enzyme (*25*). In this respect, GLX2, despite exhibiting the same coordination sphere displayed by other hydrolases of the superfamily, has been an outstanding exception regarding the metal ion dependence.

GLX2 exists as multiple isoenzymes in eukaryotes. GLX2 activity has been found both in the cytosol and in the mitochondria (*26*−*28*), suggesting a more complex physiological role than that of GLX1. In contrast, most bacteria sequenced up to date harbor a single gene copy of each of these enzymes (http://biocyc.org). *Salmonella enterica* serovar Typhimurium constitutes an exception to this common rule (*29*). While it harbors only one open reading frame coding for a GLX2 enzyme (STM0261 or *gloB*), three putative GLX1 enzymes are encoded in this pathogen's genome, including STM0235 (*yaeR*) and STM1435 (*gloA*), both present also in other *S. enterica* serovars. It also includes STM3117, a gene located in a putative pathogenicity island present only in some *Salmonella* serovars, such as Choleraesuis and Enteritidis, that encodes a virulence factor (*30*). Different intracellular pathogens, such as *Salmonella* and *Brucella*, when internalized by macrophages, employ this detoxifying system as a defense mechanism to the accumulation of methylglyoxal generated in the phagolysosome (*31*, *32*).

We report here the biochemical, structural, and biophysical characterization of GloB, the GLX2 from the pathogen *Salmonella typhimurium*. We have found that this bacterial enzyme can also employ different metal cofactors such as Fe(II), Fe(III), Zn(II), and Mn(II) to give rise to active forms, though with a clear predominance favoring iron ions. The iron form shares some spectroscopic features reported for eukaryotic homologues. On the basis of the high-resolution crystal structure of this enzyme, we also propose a rationale for the selectivity for iron of GLX2, based on the presence of conserved amino acid residues at the second shell around the metal binding sites. This preference for the iron form of the *Salmonella* enzyme, when compared to the recently characterized GLX2 from *E. coli* enzyme (*33*) in its di-Zn-(II) form, could be related to its role in pathogenicity.

EXPERIMENTAL PROCEDURES

General Information. S-D-Lactoylglutathione (SLG) was purchased from Sigma-Aldrich. All chromatographic steps were performed on an Amersham Biosciences liquid chromatography system operating at 4 °C. Metal standards were purchased from Fisher Scientific and were diluted with distilled water. All other chemicals used in this study were purchased commercially and were of the highest quality available.

Gene Amplification and Cloning. STM0261 (*gl0B*) was PCR amplified from *S. enterica* serovar Typhimurium 14028s chromosome as previously described (*34*), using the primers 0261NTF (5′-ATCGGATCCATGAATCTTAACAG-TATTCCCGCG-3′) and 0261CTR (5′-ATGCCTCGAGAA-GCTTTCAGAACGTGTCTTTCTTTGAC-3′), which include a *Bam*HI and an *Xho*I restriction site at the 5′ and 3′ ends of the fragment. The amplified 700 bp *gloB* PCR fragment was purified from a 2% agarose gel using a Qiaex (Qiagen) band purification kit and cloned between the *Bam*HI and *Xho*I restriction sites in the pKP cloning vector (a derivative of the pBluescript II vector, Stratagene). The *gloB* sequence was determined from the resulting plasmid pKP-*gloB*. *gloB* was then cloned into a pET32a(+) expression vector (Novagen), generating plasmid pET32-*gloB*. The plasmid was finally introduced into XL1-blue *E. coli* cells by electroporation using a Bio-Rad apparatus following the manufacturer's recommendations. This cloning strategy resulted in the addition of six extra residues to the N-terminus of GloB.

Protein Overexpression and Purification. The GLX2 (GloB) from *S. typhimurium* recombinantly produced in *E. coli* was used for this study. Overexpression and purification were performed using the pET32-*gloB* vector. This system yields high-level expression of the recombinant GloB protein sequence fused by its N-terminal end to the cleavable Trx·Tag thioredoxin protein and the His·Tag sequence.

Optimal induction conditions for the expression of GloB protein were achieved using isopropyl β-D-thiogalactoside (IPTG) or lactose as the inductor agent, and different temperatures of induction were attempted. Optimal overexpression of the fusion protein was achieved by inducing a BL21-(DE3)pLysS′ *E. coli* culture at OD_{600} 0.4−0.6 with 0.5 mM IPTG and growing it for 4 h at 30 °C.

In a typical protein preparation, a 2 L BL21-(DE3)pLysS′ *E. coli* culture was grown in LB medium (Sigma) and induced as described above. The bacteria were harvested by centrifugation and resuspended in 50 mM Tris−HCl, pH 8.0, 1 mM phenylmethanesulfonyl fluoride, 0.01 mg/mL DNAse, and 5 mM $MgCl_2$. Sonication was performed four times for 30 s followed by ultracentrifugation at 100000*g*. The bacterial lysate was applied to a column of Ni-agarose (Qiagen). After washing with 50 mM Tris−HCl, pH 8.0, 300 mM NaCl, and 20 mM imidazole, the fusion protein was eluted with 50 mM Tris−HCl, pH 8.0, 300 mM NaCl, and 250 mM imidazole. The fusion protein was diafiltrated using an Amicon concentrator to exchange to the buffer needed for the enterokinase digestion (50 mM Tris−HCl, pH 8.0, 10 mM $CaCl_2$). The sample was then incubated with 50 units of enterokinase protease (EKmax, Invitrogen) for 2 h at 20 °C, according to the manufacturer's instructions. After the digestion the sample was diluted 1:3 in 50 mM Tris−HCl, pH 8.0, and loaded onto the Ni-agarose column. Trx·Tag thioredoxin protein plus the His·Tag was bound to the resin, whereas the pure GloB passed through it. Fractions with GLX2 activity were pooled and dialyzed against 10 mM 4-morpholinepropanesulfonic acid (MOPS) and 0.2 M NaCl at pH 7.2.

Minimal medium M9 was employed to produce selectively metal-enriched enzyme species. The minimal medium contained 4 g/L D-(+)-glucose (Sigma), 12.8 g/L $Na_2HPO_4 \cdot 7H_2O$, 3 g/L KH_2PO_4, 0.5 g/L NaCl, 1.0 g/L ammonium sulfate, 10 μM $CaCl_2$, and 1 mM $MgSO_4$. Supplemental metal ions were added from stock solutions of $Fe(NH_4)SO_4$, $MnCl_2$, or $ZnCl_2$ to reach a final concentration in the culture of 100 μM. The metal ions were added in the moment of the induction, when the growth cultures reached an OD_{600} of 0.6−0.8.

Protein Concentration. Enzyme concentrations were determined by measuring the $A_{280\,nm}$ and using the extinction coefficient $\epsilon_{280\,nm} = 28\,030\ M^{-1}\ cm^{-1}$. This parameter was calculated from amino acid composition information by applying a modified Edelhoch method (*35*).

Steady-State Kinetics. Steady-state kinetic parameters were determined by measuring the initial rates of formation of glutathione due to the hydrolysis of SLG in the presence of 200 μM 5,5′-dithiobis(2-nitrobenzoate) (DTNB) at 412 nm ($\epsilon_{412\,nm} = 13\,600\ M^{-1}\ cm^{-1}$) as described in ref *36*. The concentration of SLG was varied from 18 to 1000 μM, and the amount of enzyme was 100−200 nM. The measurements were performed in a reaction volume of 300 μL of 10 mM MOPS, 0.2 M NaCl, pH 7.2, buffer, at 30 °C in a Jasco 550 UV−vis spectrophotometer. In the case of the enzyme obtained from minimal medium the measurements were performed with the addition of a 20 μM concentration of the corresponding metal ion (iron, zinc, or manganese) according to the metal form of the enzyme that was being measured. The measurements were performed at least in triplicate. Kinetic constants were determined by fitting the data of initial rates to the Michaelis−Menten equation.

Metal Analysis. The metal content of the GloB samples was measured using atomic absorption spectroscopy in a Metrolab 250 AA instrument. Purified enzymes were diluted with 10 mM MOPS, pH 7.2, to a concentration of 30 μM and analyzed for zinc, manganese, and iron. The metal content data presented in this paper represent an average from at least three preparations of each growth condition.

Protein Crystallization and X-ray Diffraction Data Collection. GloB purified from expression in rich growth medium was concentrated to 8.0 mg/mL and screened against Crystal Screen I and II kits (Hampton Research) with the hanging-drop vapor diffusion method at 4 and 18 °C employing equal volumes of the reservoir solution and protein. Small crystals were observed after two weeks at 4 °C in 0.1 M MES buffer, pH 6.5, 12% PEG 20 000. The crystals were cryoprotected by addition of 20% ethylene glycol to the reservoir solution.

An initial diffraction data set was collected to 1.7 Å resolution on a MAR345dtb image-plate detector using Cu Kα radiation generated by a Rigaku Ultra-X 18 rotating anode operating at 90 mA and 50 kV and focused using Osmic mirrors. Other crystals from the same crystallization batch were used to collect a 1.45 Å resolution diffraction data set at beamline MX1 in the Brazilian National Light Source (LNLS) (*37*, *38*). Diffraction data were integrated and reduced with MOSFLM (*39*), and intensities were scaled with SCALA from the CCP4 suite (*40*). Data collection statistics are summarized in Table 3.

Structure Solution, Refinement, and Validation. The molecular replacement was performed with PHASER (*41*) using the 1.7 Å data set and a search model prepared with Chainsaw (*40*) based on the crystal structure of *Arabidopsis thaliana* GLX2 (Protein Data Bank code 1XM8) (*13*). The *S. typhimurium* structure was modeled and rebuilt using COOT (*42*), and refinement was carried out against the 1.45 Å resolution data set using REFMAC5 (*43*) and PHENIX-REFINE (*44*). The structure was validated using PROCHECK (*45*), and the final data refinement statistics are shown in Table 3. All pictures were created in PyMOL (*46*). The coordinates and structure factors have been deposited in the Protein Data Bank (accession number 2QED).

^{1}H NMR Spectroscopy. NMR spectra were recorded on a Bruker Avance II 600 spectrometer operating at 600.13 MHz at different temperatures, as indicated. ^{1}H NMR spectra were recorded under conditions to optimize detection of the fast relaxing paramagnetic resonances, using either the super-WEFT pulse sequence (*47*, *48*) or water presaturation. Spectra were acquired over large spectral widths with acquisition times ranging from 16 to 80 ms and intermediate delays from 2 to 35 ms. 1D experiments with solvent presaturation were used to record isotropically shifted signals closer to the diamagnetic envelope. The samples in D_2O were made by performing three or more dilution/concentration cycles in an Amicon centrifugal filter device to a final concentration of 1.3 mM. The samples were then loaded into Wilmad 5 mm tubes for NMR.

Electron Paramagnetic Resonance Spectroscopy. X-band (9.5 GHz) EPR spectra were measured on a Bruker ELEXSYS E580 system (Bruker BioSpin, Germany) at 4.7 and 31 K. The temperature was controlled with an Oxford ITC503 cryogenic system. EPR samples containing a convenient amount of protein were frozen by immersion in liquid nitrogen and then placed in the spectrometer rectangular cavity. All EPR data were corrected by subtracting a baseline corresponding to the EPR signal of the buffer. Other acquisition conditions: modulation amplitude, 1 mT; modu-

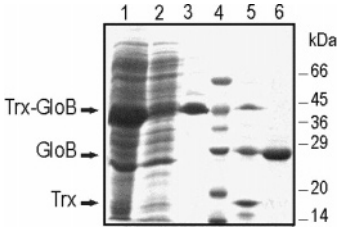

FIGURE 2: SDS−PAGE of the purification steps of GloB. The different lanes correspond to (1) the soluble fraction of the induced bacterial extract, (2) the flow-through after the wash step in a Ni-agarose affinity column, (3) elution of the 45 kDa fusion protein from this resin, (4) molecular mass standards (Sigma), (5) digestion of the fusion protein by enterokinase, and (6) purified GloB.

lation frequency, 100 kHz; microwave power, 4 mW. A typical EPR sample was 1 mM in 10 mM MOPS, pH 7.2, buffer.

RESULTS

Cloning of the gloB Gene and Protein Expression. The STM0261 gene (*gloB*) encodes a 28 kDa protein with high homology with GLX2. This gene was specifically amplified from the *S. enterica* serovar Typhimurium 14028s genome and finally cloned in an expression vector. Different expression and purification strategies were attempted. Overexpression of GloB in a pET22b plasmid gave reasonable protein yields. All attempts to purify GloB by using a glutathione-agarose resin, as reported for the yeast enzyme (*49*), were unsuccessful. Interestingly, this approach could not be applied either to the *E. coli* protein (*33*). Then we resorted to other strategies in which GloB was expressed as a fusion protein. When GloB was produced as an N-terminal or C-terminal fusion protein to GST, good levels of protein expression were obtained, but cleavage of the fusion protein with a protease gave low yields. Finally, GloB was cloned in a pET32a(+) plasmid, and the protein was overexpressed in a BL21-(DE3)pLysS′ *E. coli* culture as a fusion protein to Trx·Tag plus His·Tag (Figure 2). After sonication and ultracentrifugation, the soluble fraction of the culture was loaded onto a Ni-agarose column. Followed by the wash step, the protein was eluted with a buffer containing 250 mM imidazole. The fusion protein was then cleaved with enterokinase (EKmax). To separate GloB from the Trx·Tag plus His·Tag, the digestion sample was loaded again onto the Ni-agarose column. In this case, Trx·Tag plus His·Tag and some of the eventually nondigested fusion were retained on the resin, whereas GloB passed directly through the column. Once obtained, the pure protein was dialyzed against MOPS buffer and quantified using the molar extinction coefficient at 280 nm of 28 030 M^{-1} cm^{-1}. This successful purification procedure resulted in an average yield of 70 mg of GloB/2 L of culture.

Due to the high sequence homology between GloB and other GLX2 enzymes from different organisms and the presence of the typical metal binding site of the metallo-β-lactamase superfamily members, we assayed the hydrolytic activity of GloB against SLG. GloB was able to hydrolyze SLG, confirming its predicted identity as GLX2. This activity was impaired with the addition of EDTA to the reaction medium (data not shown).

Metal Content and Catalytic Activity of GloB. Previous studies on GLX2 have reported different metal contents for the recombinant enzymes (Table 1). In general, the wild-type forms of the recombinant GLX2 isoenzymes characterized up to now (GLX2 from *Homo sapiens* and *A. thaliana*) were isolated with significant but varying amounts of iron, zinc, and manganese bound to their active sites (*10*−*14*).

Table 1: Metal Content of GLX-2 Samples: Comparison of GLX2 Metal Contents Reported in Previous Studies with That Obtained in This Job in Similar Work Conditions

isoform	Zn	Fe	Mn	total metal content
human GLX2-2[a]	1.5	0.7	not tested	2.2
Arabidopsis GLX2-2[b]	0.4	0.8	0.30	1.5
Arabidopsis GLX2-5[c]	0.58	0.61	ND[e]	1.19
Salmonella GLX2[d]	0.21 ± 0.01	0.64 ± 0.02	0.30 ± 0.05	1.15 ± 0.28

[a] From ref *10*. [b] From ref *14*, grown in ZY medium without extra addition of metal. [c] From ref *13*, without extra added metal ion. [d] This work, grown in LB medium. [e] ND = not detected.

To study the metal content of a prokaryotic GLX2 recombinantly produced in *E. coli*, we overexpressed GloB either in a rich medium or in minimal medium supplemented with different metal ions. The identity of the metal ions bound to the protein obtained under different growth conditions was determined by atomic absorption measurements. In the case of the protein purified from LB medium, the metal content was 0.21 zinc, 0.64 iron, and 0.30 manganese per protein. These results are compared in Table 1 with those already reported for the human and *Arabidopsis* enzymes. It is clear that, as reported for the eukaryotic GLX2's, GloB is overexpressed with iron, zinc, and manganese bound. A metal occupancy lower than 2 may be attributed to a loss of metal during purification or to a limited metal availability during overexpression.

The kinetic parameters for the enzyme purified from a rich expression medium using SLG as the substrate are summarized in Table 2. The reported values are comparable to those obtained for GLX2 from other organisms. In an attempt to elucidate whether one of these metal ions is essential for the catalytic activity of GloB, we overexpressed the protein in minimal medium and supplemented it with different metal ions in the induction step. In this case, we were able to obtain different metal forms of GloB as described in Table 2. The catalytic efficiencies (k_{cat}/K_M) for the four forms of the protein were within the same order of magnitude and very close to those reported for other GLX2 family members, with a higher catalytic performance of the Mn variant. These assays revealed that GloB is able to bind the three different metal ions into its active site, yielding active forms in all cases.

Spectroscopic Studies on GloB. (1) Electron Paramagnetic Resonance. EPR spectra of GloB isolated from rich medium at 4.7 K (Figure 3A, upper trace) and 31 K (inset in Figure 3A) indicate the presence of four different sets of lines: (1) a resonance at $g_{e\ ff} \approx 9.1$, (2) resonances at $g_{eff} \approx 4.3$, (3) a six-line pattern with hyperfine splitting of ca. 8 mT and centered around $g_{eff} \approx 2.0$, and (4) a broad resonance at $g_{eff} < 2.0$. Simulations of the EPR spectrum in Figure 3A using the software EasySpin (*50*) allowed the assignment of those sets of resonances as described below.

The first two sets ($g_{eff} \approx 9.1$ and 4.3) constitute the main components in the EPR spectra and are characteristic of magnetically isolated high-spin Fe(III) in a rhombic environment (*51*−*53*). Those lines arise from the ground-state m_S

Table 2: Steady-State Kinetic Constants and Metal Content of GloB Samples[a]

	k_{cat} (s^{-1})	K_M (μM)	$k_{cat}/K_M \times 10^5$ (s^{-1}/M)	Fe/enzyme	Mn/enzyme	Zn/enzyme	total metal content
rich	168.8 ± 8.5	408 ± 50	3.5 ± 0.6	0.64 ± 0.02	0.30 ± 0.05	0.21 ± 0.01	1.15 ± 0.28
Zn-M9	209.9 ± 6.2	295 ± 27	7.1 ± 0.6	ND	ND	1.40 ± 0.02	1.40 ± 0.02
Fe-M9	149.9 ± 12.9	463 ± 10	3.2 ± 0.3	0.65 ± 0.01	ND	0.07 ± 0.01	0.72 ± 0.11
Mn-M9	394.9 ± 11.2	241 ± 18	16.4 ± 1.7	ND	1.10 ± 0.03	ND	1.10 ± 0.03

[a] Both the metal content and the steady-state kinetics were determined as described in the Materials and Methods. Values are the average standard deviation obtained from independent measurements on at least three protein preparations. "rich" corresponds to the enzyme obtained from LB medium. "Zn/Fe/Mn-M9" corresponds to the enzyme obtained from minimal medium supplemented with the different metal ions. ND = not detected.

Table 3: Crystallographic Data Collection and Refinement Statistics[a]

data set		home source	LNLS
space group		$P2_1$	$P2_1$
cell dimens	*a*, *b*, *c* (Å)	44.13, 58.37, 54.76	43.37, 57.17, 53.9
	β (deg)	112.08	111.90
wavelength (Å)		1.541	1.427
resolution (Å)		50.76 (1.67)	14.4 (1.45)
R_{merge}[b] (%)#		5.7 (32)	7.3 (31.6)
$I/\sigma(I)$		9.2 (2.3)	6.7 (1.9)
completeness (%)		98.3 (88.9)	99.9 (99.9)
redundancy		4.8 (4.5)	5.4 (5.2)
no. of obsd reflns		142 464	235 043
no. of unique reflns		29 723	43 386
Refinement			
no. of atoms			2670
R_{work}/R_{free} (%)			15.7/17.8
rmsd	bond angles (deg)		0.930
	bond lengths (Å)		0.005
Ramachandran analysis (%/no.)	most favored		91.4/202
	additional allowed		8.1/18
	general allowed		0.5/1

[a] Numbers in parentheses represent the highest resolution bin (1.53−1.45 Å). [b] $R_{merge} = \sum_h\sum_l|I_{hl} - \langle I_h\rangle|/\sum_h\sum_l\langle I_h\rangle$, where I_{hl} is the intensity of the *l*th observation of reflection *h* and $\langle I_{hl}\rangle$ are the mean intensities of the *h* reflections. R_{merge} is computed over all *l* observations of *h* reflections.

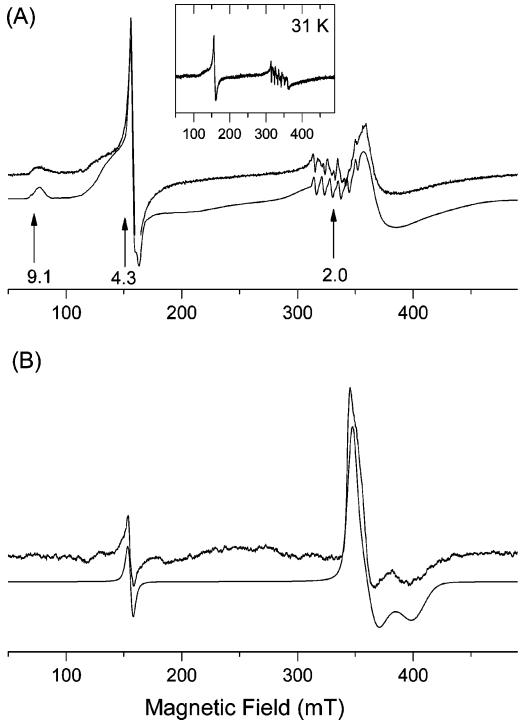

FIGURE 3: Experimental (upper traces) and calculated (lower traces) X-band EPR spectra from (A) 1 mM GloB and (B) 1 mM iron-only GloB. The inset in panel A shows the GloB spectrum measured at 31 K. The arrows indicate approximate effective *g* values.

$= \pm 1/2$ ($g_{eff} \approx 9.1$) and from the $m_S = \pm 3/2$ ($g_{eff} \approx 4.3$) states. The former states are populated only at very low temperatures, explaining why this resonance is not observed at 31 K (inset in Figure 3A). Simulation of such components using the spin Hamiltonian $H = \beta g_0 \cdot \mathbf{B} \cdot \mathbf{S} + \mathbf{S} \cdot \mathbf{D} \cdot \mathbf{S}$, where β is the Bohr magneton, **B** is the applied magnetic field, and **D** is the zero-field tensor used for $S > 1/2$ systems, resulted in a good agreement between experimental and calculated spectra (Figure 3A, lower trace) when the following parameters were used: $g_0 = 2.0$, $S = 5/2$, $D = 0.33$ cm^{-1}, and $E = 0.0645$ cm^{-1} ($E/D = 0.195$). Strains in D (ΔD) and E (ΔE) values were also needed to achieve a better fit of the experimental data ($\Delta D = 0.18$ cm^{-1} and $\Delta E = 0.033$ cm^{-1}). The agreement between calculated and experimental spectra was very sensitive to variations in these values, which enables us to estimate errors around ~10% for each parameter. The parameter values determined from our simulation are very close to those obtained by Marasinghe et al.(*13*) for mitochondrial glyoxalase II, thus suggesting similar local environments in both cases. The D value determined from our simulations (0.33 cm^{-1}) is also consistent with values obtained for other non-heme iron proteins (*54*) and indicates coordination of the Fe(III) ion to a ligand system primarily formed by oxygen and nitrogen atoms that makes D approximately 0.5 cm^{-1} (*51*, *55*). We also attempted to quantify the paramagnetic species on the basis of the integration of their calculated EPR spectra (Figure 3A, lower trace) with corrections for variations in g factors (*56*). We should however keep in mind that this is not very precise in determining spin concentrations in cases where $S > 1/2$ and multiple Kramer's doublets are populated (small D value). Using this strategy, we estimated that resonances around 9.1 and 4.3 account for ca. 80% of the total iron content detected in this EPR spectrum. On the basis of the heterogeneous metal content of this sample, these signals can be tentatively attributed to an Fe(III)/Zn(II) center, as previously observed for other metalloproteins (*13*, *14*, *57*) (see below).

The third set of resonances comprises a sextet (region around $g \approx 2$ in Figure 3A) and was simulated assuming an apparent electron spin of 1/2 ($g_{eff} = 1.99$) interacting with a nuclear spin $I = 5/2$ (calculated isotropic hyperfine interaction $A = 72$ G), characteristic of a mononuclear Mn(II) center.

Finally, the broad signal at $g < 2$ has been previously assigned to an antiferromagnetically coupled center constituted by a high-spin ($S = 5/2$) Fe(III) ion and high-spin ($S = 2$) Fe(II) ion (*13*), and similar coupled Fe(III)/Fe(II)

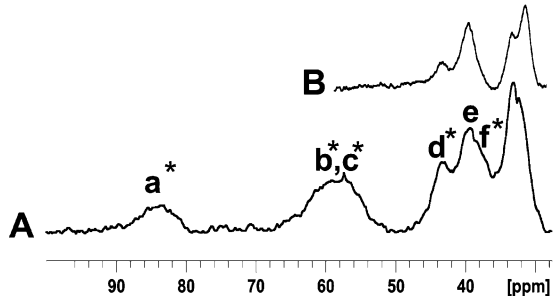

FIGURE 4: ^{1}H NMR spectra of GloB in (A) H_2O and (B) D_2O. The spectra were recorded at 600 MHz, pH 7.2, and 298 K in 10 mM MOPS buffer, 0.2 M NaCl.

binuclear sites have been observed for *A. thaliana* GLX2 (*14*) and calcineurin (*57*). This broad component is not observed in the EPR spectrum at 31 K (inset in Figure 3A), indicating a strong temperature dependence of this signal as expected for dinuclear coupled centers. Simulation of the spectrum assuming an $S = 1/2$ spin system allowed us to obtain effective g values of 1.87, 1.81, and 1.60 for this binuclear center (Figure 3A, lower trace). These g values are in good agreement with those determined for mitochondrial glyoxalase II (*13*). The use of a more detailed spin Hamiltonian, which included individual zero-field splitting for each ion and an exchange coupling, did not yield a unique set of parameters as also pointed out by Marasinghe et al. (*13*). Bearing in mind the limitations involved in quantifying the spin concentration in the present case, we determined that the broad signal at $g < 2$ accounts for roughly 20% of the total iron contributing to the EPR spectrum in Figure 3A.

The EPR spectrum of a sample of iron-only GloB (obtained from expression in minimal medium, as described above) at 4.7 K (Figure 3B, upper trace) is dominated by the signal at $g_{eff} < 2$ (associated with a coupled Fe(III)/Fe(II) center), with a concomitant decrease of the signal at $g_{eff} \approx 4.3$ corresponding to a magnetically isolated Fe(III) center. Simulation of this spectrum (Figure 3B, lower trace) led to similar effective g values (1.90, 1.83, 1.62) for the Fe(III)/Fe(II) species as compared to the simulation shown in Figure 3A (lower trace). However, line widths are somewhat narrower for the iron-only enzyme than observed for the multi-ion sample, thus leading to a better resolved spectrum (Figure 3B, lower trace). The resonance corresponding to mononuclear Fe(III) ($g_{eff} \approx 4.3$) was satisfactorily simulated with the same set of parameters employed for the previous sample. The component at 9.1 could not be detected on the basis of the low signal-to-noise ratio. The double integral of the calculated spectrum revealed that the coupled dinuclear Fe(III)/Fe(II) center represents ca. 90% of the total iron content, confirming a full metal upload in the protein expressed in minimal medium.

(2) Nuclear Magnetic Resonance. The ^{1}H NMR spectrum of GloB recorded under conditions tailored to optimize detection of the fast relaxing signals (*48*) close to a paramagnetic metal ion shows several hyperfine-shifted signals in the downfield region, up to 85 ppm (Figure 4). In this experiment, we expect to observe resonances only from iron ligands, since Mn(II) induces a considerable line broadening and yields no observable paramagnetic NMR spectrum.

The two most downfield shifted resonances, located at 84 (signal a) and 58 ppm, are absent when the spectrum is recorded in a D_2O solution. The signal envelope located at 58 ppm accounts for more than one proton, on the basis of its intensity and the fact that two partially overlapping signals can be better resolved at lower temperatures, and we label them as resonances b and c, accordingly. The signal envelope from 50 to 30 ppm includes several partially overlapping signals that are clearly sharper, but could not be resolved into individual components by changing the temperature. However, the intensity of resonances d and f at 43 and 38 ppm is decreased in the D_2O spectrum. These signals can be assigned to His metal ligands, suggesting that there are five His iron ligands. This is compatible with the presence of Fe(III) or Fe(II) ions in the two binding sites that in total bear five His ligands. This spectrum shows more signals than that reported by Marashinge et al. for the mitochondrial GLX2 from *Arabidopsis* (*13*). The narrow lines in the *Arabidopsis* enzyme have been interpreted as arising from a coupled Fe(III)/Fe(II) system. The present spectrum, despite displaying broader resonances, can only be compatible with a coupled Fe(III)/Fe(II) center. A magnetically isolated Fe(III) site (such as expected in an Fe(III)/Zn(II) center) would give rise to NMR resonances even broader (*48*, *58*), and an uncoupled Fe(II) site renders narrower signals (*59*, *60*). The NMR lines and chemical shifts are similar to those observed for purple acid phosphatases (*58*, *61*, *62*) that were shown to exhibit a weak antiferromagnetic coupling ($J \leq 10$ cm^{-1}).

The NMR spectrum of iron-only GloB (obtained as described above) was identical to the one reported in Figure 4, but with a significantly higher signal-to-noise ratio. This confirms that these resonances correspond exclusively to the coupled Fe(III)/Fe(II) form, in agreement with the EPR spectrum, which revealed an increase of the contribution of this species from 20% to 90% on going from the heterogeneous sample to the iron-only protein.

Crystal Structure of GloB. (1) Overall Structure. The structure of GloB was solved by molecular replacement using the structural data of the mitochondrial GLX2 from *A. thaliana* (*13*). The top solutions of the rotation and translation functions had a Z score of 16.2 and 16.0, respectively. The final structure was refined to an R_{work} of 15.7% and an R_{free} of 17.8% at 1.45 Å resolution (Table 3). The asymmetric unit contains 1 protein molecule, and the final model contains all residues present in the amino acid sequence, 475 water molecules, and 2 metal ions. The electron density was well defined for the whole molecule except by a short loop near the C-terminus (Leu234−Arg240), with B factors around 20.3 Å^2 against an average value of 14.5 Å^2, indicating some flexibility of this region compared to the rest of the protein.

As expected from the sequence homology, GloB shows the same protein fold observed in the *Arabidopsis* and human enzymes (*10*, *13*), with a root-mean-square deviation (rmsd) of 1.0 and 0.8 Å in the Cα positions, respectively (Figure 5A). The structure is composed by two tightly interacting domains. The N-terminal domain, which includes the first 165 residues, has the typical $\alpha\beta/\beta\alpha$ four-layer sandwich metallo-β-lactamase fold (*15*, *17*). The smaller C-terminal domain is situated at one edge of the main core and consists of five helices. This domain is typical of the GLX2 family and is considered to be essential for substrate binding (*10*, *13*, *63*).

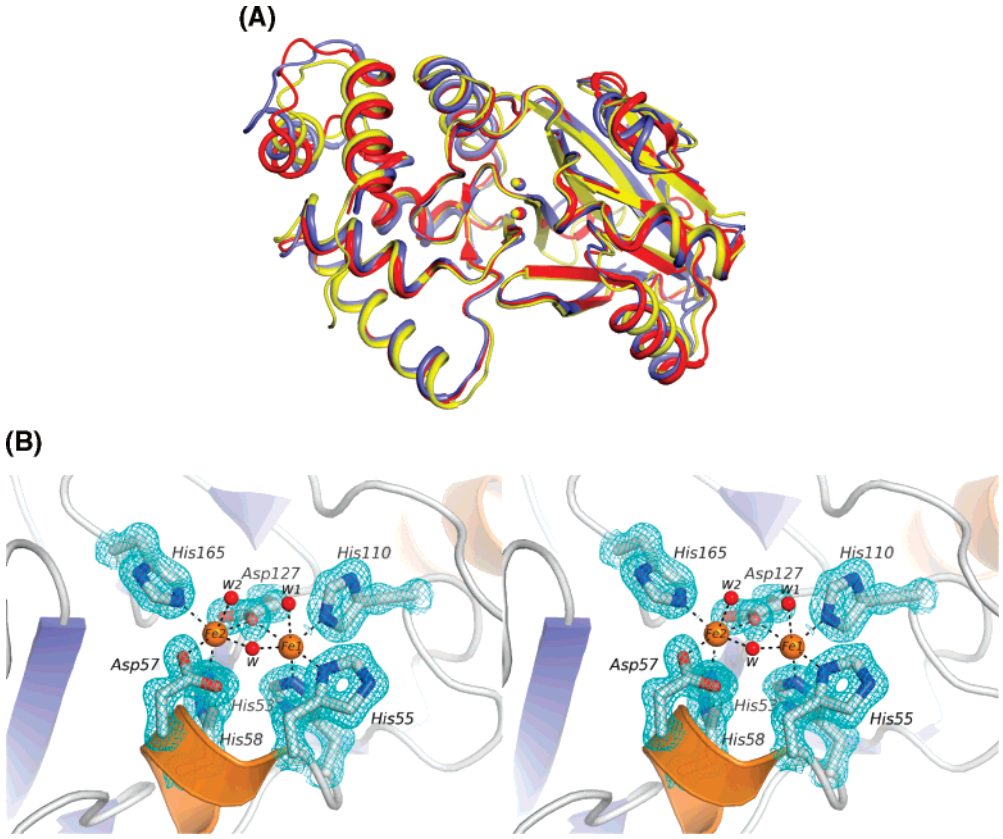

FIGURE 5: (A) Superposition of the structures of different GLX2's. The backbone traces of different glyoxalases II are shown: GloB (2QED, in blue; this work), the *Arabidopsis* mitochondrial isoform of GLX2 (1XM8, in red; *13*), and human isoenzyme (1QH5, in yellow; *10*). (B) Stereoview of the stick representation and the electron density map of the metal binding site of GloB. A H-bond network situated at the metal binding site. Fe1 is coordinated by Nϵ2@His53, Nδ1@His55, and Nϵ2@His110, while Fe2 is bound to Oδ1@Asp57, Nϵ2@His58, and Nϵ2@His165. The two metals are bridged by Oδ1@Asp127 and a water/OH molecule (W). Two water molecules (W1 and W2) are situated on the top of the metal site interacting with Fe1 and Fe2. The electron density map around the amino acids is a $|2F_o - F_c|$ map contoured at 1.5σ.

(2) Metal Site Structure. Seven protein residues and one water molecule directly interact with the two metal ions (Figure 5B). The two metals are separated by a distance of 3.3 Å and are bridged by a water molecule and the Oδ1 atom of Asp127. The identity of the metal ions cannot be unequivocally assessed from the electron density map. However, Zn(II)/Zn(II), Zn(II)/Mn(II), and Zn(II)/Fe(II) dimetallic centers are possibly less favorable since refinement attempts assuming these dinuclear centers gave rise to a strong negative signal around the density map of Zn(II) in $F_o - F_c$ even though the Zn atom occupancy is decreased. On the other hand, assumption of a diiron, a dimanganese, or a hybrid Fe/Mn center can account for the observed electron density maps; thus, none of these possibilities can be excluded. Therefore, since the metal content measurements show a predominance of iron in the active site, the final structure was refined by assuming the presence of two iron ions in its dinuclear active site. Analysis of the side chain atoms enrolled in the metal coordination showed the average *B* factor to be around 6.4 Å^2; this value is similar to those observed for Fe1 and Fe2, which were 6.97 and 6.00 Å^2, respectively. The small difference between Fe1/Fe2 *B* factors does not provide any evidence for differential occupancies for the two sites.

According to this final model, Fe1 is coordinated by His53 Nϵ2, His55 Nδ1, and His110 Nϵ2, while Fe2 is bound to Asp57 Oδ1, His58 Nϵ2, and His165 Nϵ2. All His ligands are bound through the Nϵ2 atom, except in the case of His55, in which the Nδ1 is the donor atom. This agrees with the His binding mode observed along the metallo-β-lactamase superfamily (*15*).

During the refinement, a weak electron density was located close to the active site. Different attempts to refine this density with a glutathione molecule were performed, but the low occupancy does not allow us to define the position nor the identity of this exogenous ligand. Therefore, the structure was refined with only two solvent molecules as apical metal ligands, one bound to each iron atom. The position of these water molecules is the same as occupied by the oxygen atoms of a cacodylate ion found in the structure of human GLX2 (1QH3) (*10*) and for a water molecule bound to Zn1 in the *Arabidopsis* GLX2 structure (1XM8) (*13*).

The position of the His side chains is determined by second-shell interactions, such as the hydrogen bonds subtended by the nonbinding N atom in the imidazole rings. Figure 6 shows second-shell interactions observed in the present structure. The carboxylate moiety of Asp28 is oriented in such a way that its Oδ2 is within H-bonding distance of the Nδ1 atom of His58 (2.71 Å), while its Oδ1 atom is located 2.71 Å from the backbone nitrogen of Thr52. Since Thr52 acts as a second-shell ligand of His53, with its Oγ1 as a H-bond acceptor from the His53 Nδ1 atom, Asp28 seems to play an essential role in building the structure of the metal site by orienting one His ligand from each of the two metal binding sites. His110 forms a H-bond through its Nδ1 and the main chain carbonyl oxygen from Arg136.

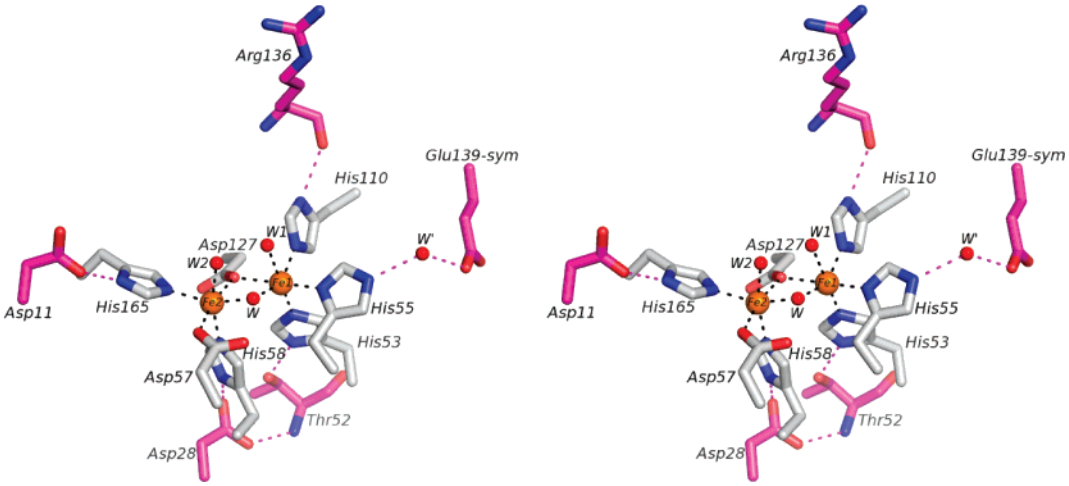

FIGURE 6: Schematic stereoview of the second-shell amino acid ligands of the metal binding site of GloB. The metal ions are shown as golden spheres. The metal ligands are colored in CPK mode, while carbon atoms from second-shell ligands are shown in purple. Metal−ligand bonds are shown as black dashed lines, while H-bonding interactions are shown as purple dashed lines.

Table 4: Differences in the Second-Shell Ligand Set among Structurally Characterized MBL Superfamily Members[a]

PDB coordinates	metal ion	His ligand	metal−ligand distance (Å)	second-sphere ligand (distance, Å)
2QED	Fe2	Nϵ2@His165	2.08	Oδ1@Asp11 (2.80)
1QH5	Zn2	Nϵ2@His173	2.13	Oδ1@Asp11 (3.02)
1XM8	Fe2	Nϵ2@His169	2.00	Oδ1@Asp11 (2.89)
2BR6	Zn2	Nϵ2@His235	2.20	O@Pro34 (2.66)
1Y44	Zn2	Nϵ2@His269	2.29	Oγ1@Thr233 (2.97)
1P9E	Zn2	Nϵ2@His302	2.18	O@Ser96 (2.80)

[a] The PDB files correspond to the following enzymes: 2QED (GloB from *S. typhymurium*; this work), 1QH5 (human GLX2; *10*), 1XM8 (*A. thaliana* GLX2; *13*), 2BR6 (homoserine lactone hydrolase; *23*), 1Y44 (tRNaseZ; *65*), 1P9E (methylparathion hydrolase; *22*). The residue numbering of each protein has been maintained. The compared His ligand is homologous for all examined enzymes. The second-sphere ligands are residues forming a H-bond with the noncoordinating His Nδ1 atom.

Instead, His55 H-bonds to a solvent molecule that on its turn interacts with Oϵ2 from Glu139. Finally, His165 is oriented by an interaction with the Oδ1 from Asp11. Asp11 plays the same role in all studied GLX2's and seems to be unique to these enzymes, since it is not conserved in other members of the metallo-β-lactamase superfamily (Table 4 and Table 1 in the Supporting Information).

(3) Substrate Binding Site. The crystal structure of human GLX2 complexed with glutathione and *S*-[(hydroxybromophenyl)carbamoyl]glutathione showed that an arginine residue, two lysine residues, and two tyrosine residues (Arg249, Lys252, Lys143, Tyr175, and Tyr145 in the human GLX2 sequence (*10*)) are within 13 Å of Zn1 and interact with these ligands. These residues involved in substrate binding in human GLX2 are conserved in GloB, except for Tyr145 and Lys143, which are substituted by a Phe and Arg residue, respectively (Phe138 and Arg136 in the GloB sequence). In the structure of the complexed human enzyme, the phenolic OH@Tyr145 interacts with a carbonyl group from glutathione. This interaction cannot be possible when this residue is replaced by a Phe in GloB. Multiple sequence alignment of different glyoxalases II reveals that an aromatic residue is fully conserved in this position in all enzymes. GLX2's from mammals are unique in harboring a Tyr residue in this position, while the rest (including prokaryotic, fungal, plant, and yeast enzymes) possess a Phe residue. We therefore conclude that this interaction is not essential for substrate recognition, yet the residue substitution among different species remains an interesting issue to solve.

DISCUSSION

In this work we have accomplished a structural and biochemical characterization of GloB, the GLX2 from *S. typhimurium*. This enzyme recombinantly produced in *E. coli* was isolated with significant amounts of iron, manganese, and zinc bound to its active site, with a clear preference toward iron. Recombinant GloB displayed similar catalytic efficiencies with different ratios of active site bound iron, manganese, and zinc. This feature is indicative of certain flexibility of the active site of GloB to accommodate any of these metal ions and to carry out the hydrolytic reaction with similar efficiency in all cases. The Mn-only variant displays a somehow larger catalytic efficiency and k_{cat} values. Interestingly, the recently characterized GLX2 from *E. coli*, originally isolated in the dizinc form, also shows a high activity in the reconstituted Mn(II) form (*33*).

EPR spectroscopy reveals the presence of a magnetically uncoupled Fe(III) center, a magnetically spin coupled Fe(III)/Fe(II) center, and an uncoupled Mn(II) center, thus indicating that a range of metal−metal combinations are incorporated during the overexpression. NMR data are consistent with the presence of an Fe(III)/Fe(II) center with a weak antiferromagnetic coupling. This is in agreement with the crystal structure that shows a bridged dimetallic center. The EPR and NMR spectra of the Fe-only sample obtained by expression in minimal medium supplemented with iron reveal that this enzyme harbors exclusively a coupled Fe(III)/Fe(II) dinuclear site.

The binding of different metal ions may be a consequence of the overexpression of this protein in *E. coli* and may not represent the physiologically active metal-loaded species. One possible explanation for this observation is that a limited metal availability during overexpression forces the nascent polypeptide to bind other metals in addition to the native one. Another hypothesis could be that GLX2 employs different metal uptake machinery on its native environment that is lacking in the heterologous host. This hypothesis could

explain the behavior observed in the eukaryotic proteins, but may not hold for a *Salmonella* protein overexpressed in *E. coli*. Finally, overexpression of different members of the metallo-β-lactamase superfamily yields exclusively Zn(II) variants, GLX2 being the only exception. This strongly suggests that there must be other features related to the enzyme itself to explain the preference for iron and the metal ion promiscuity.

The immediate environment of metal sites in metalloproteins determines the selectivity in the metal ion uptake (*64*). A detailed inspection of the enzyme metal site compared to that in other systems reveals that the metal binding site of GLX2 is identical to that found in different members of the superfamily that have been characterized as Zn-only proteins, such as phosphodiesterase (*19*), acyl-homoserine-lactone lactonase (*20*, *23*, *24*), methylparathion hydrolase, and alkylsulfatase (*21*). Instead, some differences arise in analysis of the second-shell amino acid ligands (Table 4, Figure 6, and Table 1 in the Supporting Information). Asp11 forms a strong H-bond with His165, a Site2 ligand. This residue is conserved in all known GLX2's, but is replaced by Thr or Ser residues in other superfamily members. An Asp residue in this position is expected to increase the hardness of the metal binding site (favoring iron uptake), as well as the negative charge of the ligand set, favoring binding of trivalent cations to the active site. We therefore propose that this second-shell amino acid ligand favors iron uptake in GLX2. Interestingly, both GLX1 and GLX2 enzymes display a subtle control of metal ion recognition. However, the metal ion requirements (either Ni(II) or Zn(II)) are strict among GLX1's, while GLX2's seem to show no preference regarding the different metal cations to render a preferentially more active enzyme.

The present study shows that bacterial GLX2's are active as diiron enzymes. The isolation of *E. coli* GLX2 (which displays a 78% sequence identity with GloB) as a dizinc enzyme is reported in a recent work. The study of the iron variant of the *E. coli* enzyme, which has not been characterized yet, would provide considerable insight into the understanding of metal dependence among prokaryotic glyoxalases II. Although the role of GloB in *Salmonella* pathogenesis has not yet been studied, a recent report showed that STM3117 (coding for a GLX1) contributes to the replication of the pathogen inside macrophages (*30*). Thus, the glyoxalase system is expected to play an important role in the survival of the pathogen under these conditions. Fe(II) concentrations above 5−10 μM have been reported (*31*) to provide an appropriate environment for the metal uptake event of this enzyme.

These observations, together with the presence of two other homologous genes coding for GLX1 isoenzymes in *Salmonella* allow us to postulate that proper methylglyoxal processing would play a major role in *Salmonella*'s survival, probably both inside and outside the host. It is possible that these three enzymes would display differential substrate selectivity. Since it is expected that GloB will second STM3117 in the methylglyoxal pathway, a direct correlation of the *Salmonella* GLX2 in virulence can be predicted.

ACKNOWLEDGMENT

We thank Dr. R. Girolami for atomic absorption measurements.

SUPPORTING INFORMATION AVAILABLE

A table listing the first- and second-shell ligands commonly found in some representative members of the metallo-β-lactamase superfamily. This material is available free of charge via the Internet at http://pubs.acs.org.

REFERENCES

1. Thornalley, P. J. (1993) The glyoxalase system in health and disease, *Mol. Aspects Med. 14*, 287−371.
2. Thornalley, P. J. (1998) Glutathione-dependent detoxification of alpha-oxoaldehydes by the glyoxalase system: involvement in disease mechanisms and antiproliferative activity of glyoxalase I inhibitors, *Chem.-Biol. Interact. 111*−*112*, 137−151.
3. Ferguson, G. P., Totemeyer, S., MacLean, M. J., and Booth, I. R. (1998) Methylglyoxal production in bacteria: suicide or survival? *Arch. Microbiol. 170*, 209−218.
4. Kalapos, M. P. (1999) Methylglyoxal in living organisms: chemistry, biochemistry, toxicology and biological implications, *Toxicol. Lett. 110*, 145−175.
5. Thornalley, P. J. (1996) Pharmacology of methylglyoxal: formation, modification of proteins and nucleic acids, and enzymatic detoxification−a role in pathogenesis and antiproliferative chemotherapy, *Gen. Pharmacol. 27*, 565−573.
6. Clugston, S. L., Barnard, J. F., Kinach, R., Miedema, D., Ruman, R., Daub, E., and Honek, J. F. (1998) Overproduction and characterization of a dimeric non-zinc glyoxalase I from Escherichia coli: evidence for optimal activation by nickel ions, *Biochemistry 37*, 8754−8763.
7. Sukdeo, N., Clugston, S. L., Daub, E., and Honek, J. F. (2004) Distinct classes of glyoxalase I: metal specificity of the Yersinia pestis, Pseudomonas aeruginosa and Neisseria meningitidis enzymes, *Biochem. J. 384*, 111−117.
8. Creighton, D. J., and Hamilton, D. S. (2001) Brief history of glyoxalase I and what we have learned about metal ion-dependent, enzyme-catalyzed isomerizations, *Arch. Biochem. Biophys. 387*, 1−10.
9. Armstrong, R. N. (2000) Mechanistic diversity in a metalloenzyme superfamily, *Biochemistry 39*, 13625−13632.
10. Cameron, A. D., Ridderstrom, M., Olin, B., and Mannervik, B. (1999) Crystal structure of human glyoxalase II and its complex with a glutathione thiolester substrate analogue, *Struct. Folding Des. 7*, 1067−1078.
11. Zang, T. M., Hollman, D. A., Crawford, P. A., Crowder, M. W., and Makaroff, C. A. (2001) Arabidopsis glyoxalase II contains a zinc/iron binuclear metal center that is essential for substrate binding and catalysis, *J. Biol. Chem. 276*, 4788−4795.
12. Wenzel, N. F., Carenbauer, A. L., Pfiester, M. P., Schilling, O., Meyer-Klaucke, W., Makaroff, C. A., and Crowder, M. W. (2004) The binding of iron and zinc to glyoxalase II occurs exclusively as di-metal centers and is unique within the metallo-beta-lactamase family, *J. Biol. Inorg. Chem. 9*, 429−438.
13. Marasinghe, G. P., Sander, I. M., Bennett, B., Periyannan, G., Yang, K. W., Makaroff, C. A., and Crowder, M. W. (2005) Structural studies on a mitochondrial glyoxalase II, *J. Biol. Chem. 280*, 40668−40675.
14. Schilling, O., Wenzel, N., Naylor, M., Vogel, A., Crowder, M., Makaroff, C., and Meyer-Klaucke, W. (2003) Flexible metal binding of the metallo-beta-lactamase domain: glyoxalase II incorporates iron, manganese, and zinc in vivo, *Biochemistry 42*, 11777−11786.
15. Daiyasu, H., Osaka, K., Ishino, Y., and Toh, H. (2001) Expansion of the zinc metallo-hydrolase family of the beta-lactamase fold, *FEBS Lett. 503*, 1−6.
16. Gomes, C. M., Frazao, C., Xavier, A. V., LeGall, J., and Teixeira, M. (2002) Functional control of the binuclear metal site in the metallo-beta- lactamase-like fold by subtle amino acid replacements, *Protein Sci. 11*, 707−712.
17. Carfi, A., Pares, S., Duee, E., Galleni, M., Duez, C., Frère, J. M., and Dideberg, O. (1995) The 3-D structure of a zinc metallo-beta-lactamase from Bacillus cereus reveals a new type of protein fold, *EMBO J. 14*, 4914−4921.
18. Crowder, M. W., Spencer, J., and Vila, A. J. (2006) Metallo-beta-lactamases: Novel Weaponry for Antibiotic Resistance in Bacteria, *Acc. Chem. Res. 39*, 721−728.

19. Vogel, A., Schilling, O., Niecke, M., Bettmer, J., and Meyer-Klaucke, W. (2002) ElaC encodes a novel binuclear zinc phosphodiesterase, *J. Biol. Chem. 277*, 29078−29085.
20. Thomas, P. W., Stone, E. M., Costello, A. L., Tierney, D. L., and Fast, W. (2005) The quorum-quenching lactonase from Bacillus thuringiensis is a metalloprotein, *Biochemistry 44*, 7559−7569.
21. Hagelueken, G., Adams, T. M., Wiehlmann, L., Widow, U., Kolmar, H., Tummler, B., Heinz, D. W., and Schubert, W. D. (2006) The crystal structure of SdsA1, an alkylsulfatase from Pseudomonas aeruginosa, defines a third class of sulfatases, *Proc. Natl. Acad. Sci. U.S.A. 103*, 7631−7636.
22. Dong, Y. J., Bartlam, M., Sun, L., Zhou, Y. F., Zhang, Z. P., Zhang, C. G., Rao, Z., and Zhang, X. E. (2005) Crystal structure of methyl parathion hydrolase from Pseudomonas sp. WBC-3, *J. Mol. Biol. 353*, 655−663.
23. Kim, M. H., Choi, W. C., Kang, H. O., Lee, J. S., Kang, B. S., Kim, K. J., Derewenda, Z. S., Oh, T. K., Lee, C. H., and Lee, J. K. (2005) The molecular structure and catalytic mechanism of a quorum-quenching N-acyl-L-homoserine lactone hydrolase, *Proc. Natl. Acad. Sci. U.S.A. 102*, 17606−17611.
24. Liu, D., Lepore, B. W., Petsko, G. A., Thomas, P. W., Stone, E. M., Fast, W., and Ringe, D. (2005) Three-dimensional structure of the quorum-quenching N-acyl homoserine lactone hydrolase from Bacillus thuringiensis, *Proc. Natl. Acad. Sci. U.S.A. 102*, 11882−11887.
25. Frazao, C., Silva, G., Gomes, C. M., Matias, P., Coelho, R., Sieker, L., Macedo, S., Liu, M. Y., Oliveira, S., Teixeira, M., Xavier, A. V., Rodrigues-Pousada, C., Carrondo, M. A., and Le, Gall, J. (2000) Structure of a dioxygen reduction enzyme from Desulfovibrio gigas, *Nat. Struct. Biol. 7*, 1041−1045.
26. Bito, A., Haider, M., Hadler, I., and Breitenbach, M. (1997) Identification and phenotypic analysis of two glyoxalase II encoding genes from Saccharomyces cerevisiae, GLO2 and GLO4, and intracellular localization of the corresponding proteins, *J. Biol. Chem. 272*, 21509−21519.
27. Maiti, M. K., Krishnasamy, S., Owen, H. A., and Makaroff, C. A. (1997) Molecular characterization of glyoxalase II from Arabidopsis thaliana, *Plant Mol. Biol. 35*, 471−481.
28. Cordell, P. A., Futers, T. S., Grant, P. J., and Pease, R. J. (2004) The Human hydroxyacylglutathione hydrolase (HAGH) gene encodes both cytosolic and mitochondrial forms of glyoxalase II, *J. Biol. Chem. 279*, 28653−28661.
29. McClelland, M., Sanderson, K. E., Spieth, J., Clifton, S. W., Latreille, P., Courtney, L., Porwollik, S., Ali, J., Dante, M., Du, F., Hou, S., Layman, D., Leonard, S., Nguyen, C., Scott, K., Holmes, A., Grewal, N., Mulvaney, E., Ryan, E., Sun, H., Florea, L., Miller, W., Stoneking, T., Nhan, M., Waterston, R., and Wilson, R. K. (2001) Complete genome sequence of Salmonella enterica serovar Typhimurium LT2, *Nature 413*, 852−856.
30. Shi, L., Adkins, J. N., Coleman, J. R., Schepmoes, A. A., Dohnkova, A., Mottaz, H. M., Norbeck, A. D., Purvine, S. O., Manes, N. P., Smallwood, H. S., Wang, H., Forbes, J., Gros, P., Uzzau, S., Rodland, K. D., Heffron, F., Smith, R. D., and Squier, T. C. (2006) Proteomic analysis of Salmonella enterica serovar typhimurium isolated from RAW 264.7 macrophages: identification of a novel protein that contributes to the replication of serovar typhimurium inside macrophages, *J. Biol. Chem 281*, 29131−29140.
31. Eriksson, S., Lucchini, S., Thompson, A., Rhen, M., and Hinton, J. C. (2003) Unravelling the biology of macrophage infection by gene expression profiling of intracellular Salmonella enterica, *Mol. Microbiol. 47*, 103−118.
32. Eskra, L., Canavessi, A., Carey, M., and Splitter, G. (2001) Brucella abortus genes identified following constitutive growth and macrophage infection, *Infect. Immun. 69*, 7736−7742.
33. O'young, J., Sukdeo, N., and Honek, J. F. (2007) Escherichia coli glyoxalase II is a binuclear zinc-dependent metalloenzyme, *Arch. Biochem. Biophys. 459*, 20−26.
34. Checa, S. K., Espariz, M., Audero, M. E., Botta, P. E., Spinelli, S. V., and Soncini, F. C. (2007) Bacterial sensing of and resistance to gold salts, *Mol. Microbiol. 63*, 1307−1318.
35. Gill, S. C., and von Hippel, P. H. (1989) Calculation of protein extinction coefficients from amino acid sequence data, *Anal. Biochem. 182*, 319−326.
36. Ridderstrom, M., Saccucci, F., Hellman, U., Bergman, T., Principato, G., and Mannervik, B. (1996) Molecular cloning, heterologous expression, and characterization of human glyoxalase II, *J. Biol. Chem. 271*, 319−323.
37. Polikarpov, I., Perles, L. A., de Oliveira, R. T., Oliva, G., Castellano, E. E., Garratt, R. C., and Craievich, A. (1998) Set-up and Experimental Parameters of the Protein Crystallography Beamline at the Brazilian National Synchrotron Laboratory, *J. Synchrotron Radiat. 5*, 72−76.
38. Polikarpov, I., Oliva, G., Castellano, E. E., Garratt, R. C., Arruda, P., Leite, A., and Craievich, A. (1997) The protein crystallography beamline at LNLS, the Brazilian National Synchrotron Light Source, *Nucl. Instrum. Methods, A 405*, 159−164.
39. Leslie, A. G. W. (1992) Recent changes to the MOSFLM package for processing film and image data, *Jt. CCCP4 ESF-EADBM Newsl. Protein Crystallogr. 26*, 27−33.
40. Collaborative Computational Project Number 4 (1994) The CCP4 Suite: Programs for Protein Crystallography, *Acta Crystallogr., D: Biol. Crystallgor. 50*, 760−763.
41. Read, R. J. (2001) Pushing the boundaries of molecular replacement with maximum likelihood, *Acta Crystallogr., D: Biol. Crystallogr. 57*, 1373−1382.
42. Emsley, P., and Cowtan, K. (2004) Coot: model-building tools for molecular graphics, *Acta Crystallogr., D: Biol. Crystallogr. 60*, 2126−2132.
43. Murshudov, G. N., Vagin, A. A., and Dodson, E. J. (1997) Refinement of macromolecular structures by the maximum-likelihood method, *Acta Crystallogr., D: Biol. Crystallogr. 53*, 240−255.
44. Afonine, P. V., Grosse-Kunstleve, R. W., and Adams, P. D. (2005) *Acta Crystallogr., D: Biol. Crystallogr. 61*, 850−855.
45. Laskowski, R. A., MacArthur, M. W., Moss, D. S., and Thornton, J. M. (1993) PROCHECK: a program to check the stereochemical quality of protein structures, *J. Appl. Crystallogr. 26*, 283−291.
46. DeLano, W. L. (2002) *The PyMOL Molecular Graphics System*, DeLano Scientific, San Carlos, CA.
47. Inubushi, T., and Becker, E. D. (1983) Efficient detection of paramagnetically shifted NMR resonances by optimizing the WEFT pulse sequence, *J. Magn. Reson. 51*, 128−133.
48. Bertini, I., Turano, P., and Vila, A. J. (1993) NMR of paramagnetic metalloproteins, *Chem. Rev. 93*, 2833−2932.
49. Bito, A., Haider, M., Briza, P., Strasser, P., and Breitenbach, M. (1999) Heterologous expression, purification, and kinetic comparison of the cytoplasmic and mitochondrial glyoxalase II enzymes, Glo2p and Glo4p, from Saccharomyces cerevisiae, *Protein Expr. Purif. 17*, 456−464.
50. Stoll, S., and Schweiger, A. (2006) Easy Spin, a Comprehensive Software Package for Spectral Simulation and Analysis in EPR, *J. Magn. Reson. 178*, 42−55.
51. Wickman, H. H., Klein, M. P., and Shirley, D. A. (1965) Paramagnetic Resonance of Fe^{3+} in Polycrystalline Ferrichrome A, *J. Chem. Phys. 43*, 2113−2117.
52. Dowsing, R. D., and Gibson, J. F. (1969) Electron Spin Resonance of High-Spin d^5 Systems, *J. Chem. Phys. 50*, 294−303.
53. Aasa, R. (1970) Powder Line Shape in the Electron Paramagnetic Resonance Spectra of High-Spin Ferric Complexes, *J. Chem. Phys. 52*, 3919−3930.
54. Pinkowitz, R. A., and Aisen, P. (1972) Zero-field splittings of ***iron** complexes of transferrins, *J. Biol. Chem. 247*, 7830−7834.
55. Aasa, R., Carlsson, K. E., Reyes, L. S. A., and Vanngard, T. (1966) Fine and hyperfine structure in electron spin resonance spectrum of Fe3+ in ethylenediaminetetraacetic acid (EDTA), *Arch. Kemi 25*, 285−291.
56. Pilbrow, J. R. (1990) *Transition Ion Electron Paramagnetic Resonance*, Clarendon Press, Oxford.
57. Yu, L., Haddy, A., and Rusnak, F. (1995) Evidence that Calcineurin accomodates an Active Site Binuclear Metal Center, *J. Am. Chem. Soc. 117*, 10147−10148.
58. Lauffer, R. B., Antanaitis, B. C., Aisen, P., and Que, L., Jr. (1983) 1H-NMR studies of porcine uteroferrin, *J. Biol. Chem. 258*, 14212−14218.
59. Sorkin, D. L., and Miller, A. F. (2000) Amino acid-specific isotopic labeling and active site NMR studies of iron(II)- and iron(III)-superoxide dismutase from Escherichia coli, *J. Biomol. NMR 17*, 311−322.
60. Sorkin, D. L., and Miller, A. F. (1997) Spectroscopic measurement of a long-predicted active site pK in iron-superoxide dismutase from Escherichia coli, *Biochemistry 36*, 4916−4924.
61. Wang, Z., Ming, L. J., Que, L., Jr., Vincent, J. B., Crowder, M. W., and Averill, B. A. (1992) 1H-NMR and NOE studies of the purple acid phosphatases from porcine uterus and bovine spleen, *Biochemistry 31*, 5263−5268.

62. Scarrow, R. C., Pyrz, J. W., and Que, L., Jr. (1990) NMR studies of the dinuclear iron site in reduced uteroferrin and its oxoanion complexes, *J. Am. Chem. Soc. 112*, 657−665.

63. Park, H. S., Nam, S. H., Lee, J. K., Yoon, C. N., Mannervik, B., Benkovic, S. J., and Kim, H. S. (2006) Design and evolution of new catalytic activity with an existing protein scaffold, *Science 311*, 535−538.

64. Dudev, T., and Lim, C. (2003) Principles governing Mg, Ca, and Zn binding and selectivity in proteins, *Chem. Rev. 103*, 773−788.

65. de la Sierra-Gallay, I. L., Pellegrini, O., and Condon, C. (2005) Structural basis for substrate binding, cleavage and allostery in the tRNA maturase RNase Z, *Nature 433*, 657−661.

BI7007245